Beat-less algorithm based on dual-frequency compensation in railway traction applications

Shen, Lailai; Chen, Jie; Kuang, Yang; Qiu, Ruichang; Zhou, Dao; Wu, Chao; Liu, Zhigang

Published in:
IET Power Electronics

DOI (link to publication from Publisher):
10.1049/pel2.12164

Publication date:
2021

Document Version
Publisher's PDF, also known as Version of record

Received: 25 January 2021 | Revised: 5 May 2021 | Accepted: 21 June 2021

IET Power Electronics

DOI: 10.1049/pel2.12164

The Institution of Engineering and Technology WILEY

ORIGINAL RESEARCH PAPER

Beat-less algorithm based on dual-frequency compensation in railway traction applications

Lailai Shen[1] | **Jie Chen**[1] | **Yang Kuang**[2] | **Ruichang Qiu**[1] | **Dao Zhou**[3] | **Chao Wu**[3] | **Zhigang Liu**[4]

[1] School of Electrical Engineering, Beijing Jiaotong University, Beijing, China

[2] CRRC Changchun Railway Vehicles Co., Ltd., Changchun, China

[3] Department of Energy Technology, Aalborg University, Aalborg, Denmark

[4] Beijing Electrical Engineering Technology Research Center, Beijing Jiaotong University, Beijing, China

Correspondence
Jie Chen, Beijing Jiaotong University No. 3 Shangyuancun, Haidian District Beijing 100044 P. R. China.
Email: jiechen@bjtu.edu.cn

Funding information
Fundamental Research Funds for the Central Universities, Grant/Award Number: 2019YJS175

Abstract

The beat phenomenon can be a critical issue in railway traction applications. This paper proposes a dual-frequency compensation (DFC) method for the beat-less algorithm to shift the spectrum of the beat voltages to a higher-frequency region. Two variables for frequency compensation are derived by mathematical calculations based on the single-frequency compensation (SFC) method. The applicability and superiority of the DFC method are analyzed. It is proposed that the DFC method can be a transition between the modulation index compensation (MIC) method and the SFC method, so the beat phenomenon can be greatly suppressed in the full speed range. The implementation of the DFC method is proposed to guide how to generate the two variables. The experimental verification is carried out on the StarSim hardware-in-loop platform, and the results demonstrate that the DFC method is more effective compared with the SFC method for beat phenomenon suppression. It also shows the modulation index with the DFC method is higher than that with the MIC method.

1 | INTRODUCTION

The AC–DC–AC traction drive system has been widely used in the electric-multiple-unit (EMU) for high reliability, high power density, and low maintenance cost. As shown in Figure 1, a typical traction drive system consists of the front-end traction transformer, the single-phase four-quadrant converter (4QC), the DC-link capacitor, the three-phase voltage source inverter, and the motors [1]. As the traction drive system is fed by the single-phase power source, the instantaneous power will fluctuate at twice the grid frequency inevitably, resulting in the DC-link voltage fluctuating at the same low frequency [2]. Coupled with such fluctuating DC-link voltage in pulse width modulation (PWM) process, the phase voltage of the inverter will contain additional subharmonic components (i.e. beat voltage). Thus, the motors will suffer from the beat phenomenon, featuring undesired current harmonics, torque pulsation, and power loss [3]. Consequently, it seriously deteriorates the safety and stability of the traction drive system.

To suppress the beat phenomenon, the passive *LC* resonant filter tuning at twice the grid frequency is installed in the DC-link for EMUs. Thereby, the fluctuating power is absorbed, and the DC-link voltage can be smooth without the low-frequency component [4]. However, the hardware solution using the *LC* resonant filter is of low power density and low reliability [5,6]. Therefore, more efforts have been made on the software solutions to remove the bulky *LC* resonant filter.

The basic idea of the software solutions is to design a special beat-less algorithm for the inverter-motor control system; hence, the phase voltage of the inverter is modified to cancel out the beat component. In [7, 8], the one-cycle control is proposed to solve the beat issue based on the volt-second area balance principle. Unfortunately, its performance is challenging with low switching frequency because the pulse sequence cannot be optimized [9, 10]. In [11, 12], the closed-loop control strategies are designed to achieve the current reference tracking without error; thus, the modulation signals for PWM process can be modified automatically, and the beat phenomenon

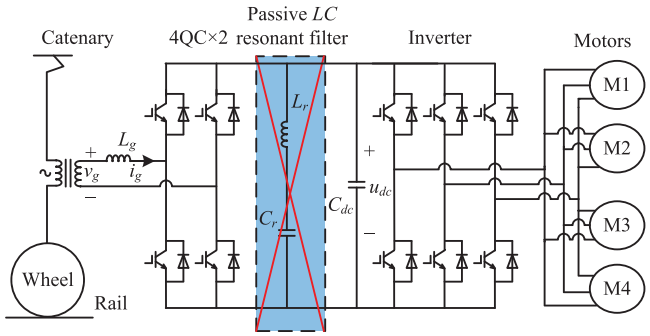

FIGURE 1 The AC–DC–AC traction drive system

can be suppressed. However, the suppression effect of these control strategies depends on the control bandwidth of the system. As for the traction drive system, where the switching frequency is low, the control bandwidth is strongly limited [13, 14]. Therefore, the current closed-loop control cannot be applied in such applications.

To get rid of the limitation of high control bandwidth, the modulation index compensation (MIC) [15, 16] and single-frequency compensation (SFC) [17–19] methods are proposed to modify the modulation signals directly. With the MIC method, the modulation index is varied against the actual DC-link voltage inversely [20, 21]. Hence, after PWM process, the phase voltage of the inverter is equivalent to the desired voltage in each switching cycle. Therefore, the subharmonics coupled by the DC-link voltage ripple will be eliminated totally if the compensation method is accurate enough [15]. However, the linear modulation region can be narrower as the maximum value of the modulation index is strongly limited in the high-speed range, especially with a large DC-link voltage ripple. Unlike the MIC method, the SFC method is more attractive because it has no such modulation index limitation in the full speed range [22]. As one variable related to the DC-link voltage is used for frequency compensation, the low-frequency beat voltage is suppressed [23–25]. However, the key drawback of the SFC method is that the amplitude of the high-frequency beat voltage will be doubled. Therefore, the beat phenomenon suppression effect can be worse compared with the MIC method. In practice, it is common to use the MIC method and the SFC method in different speed ranges for better traction performance. Nevertheless, the performance can still be further improved.

In this paper, a dual-frequency compensation (DFC) method is proposed to modify the modulation signals for beat phenomenon suppression in railway applications. Unlike the SFC method, two variables are used for frequency compensation, therefore both the low and high-frequency beat voltage can be eliminated. In regard to the modulation index, the DFC method can be superior to the MIC method. Therefore, the DFC method can be a transition between the MIC and SFC methods in the middle-speed range. Consequently, the beat phenomenon can be further suppressed in the full speed range. These two variables used for the DFC method are derived by mathematical calculations in detail. The calculation results indicate that the spectrum of the beat voltage can be shifted to a higher-frequency region. Furthermore, the trajectories of the modified modulation signal show that these three methods can be applied under different modulation indexes, and the DFC method can be more effective with a large fluctuation in the DC-link. The experimental results verified the superiority and applicability of the DFC method.

The rest of this paper is organized as follows: In Section 2, the DC-link voltage and the beat phenomenon are analyzed in detail. In Section 3, the DFC method is proposed, and its applicability, superiority, and implementation are presented. In Section 4, the experimental results are given. Finally, Section 5 draws the conclusion.

2 | BEAT PHENOMENON ANALYSIS

2.1 | DC-link voltage without LC resonant filter

The input voltage v_g and current i_g of 4QC have a sinusoidal shape, so the input power p_{in} to the traction drive system can be expressed as

$$\begin{aligned} p_{in} &= v_g i_g - L_g \frac{di_g}{dt} i_g \\ &= V_g I_g [1 - \cos(2\omega_g t)] - \omega_g L_g I_g^2 \sin(2\omega_g t) \end{aligned} \tag{1}$$

where V_g and I_g are the root mean square value (RMS) of the input voltage and current, ω_g is the angular frequency (100π) of the grid, and L_g is the grid-side inductance.

p_{in} consists of the DC power P_d and the undesired fluctuating AC power $p_{2\text{-}ripple}$, derived as follows:

$$P_d = V_g I_g \tag{2}$$

$$p_{2-ripple} = P_{2-peak} \sin(2\omega_g t + \delta) \tag{3}$$

where

$$P_{2-peak} = \sqrt{(V_g I_g)^2 + (\omega_g L_g I_g^2)^2} \quad \delta = \tan^{-1}\left(\frac{V_g}{\omega_g L_g I_g}\right)$$

Assuming that all the DC power P_d is supplied to the load, it can be known that the fluctuating AC power $p_{2\text{-}ripple}$ will flow into the DC-link capacitor C_{dc} (ignoring the power loss), that is:

$$p_{2-ripple} = C_{dc} \frac{du_{dc}}{dt} u_{dc} \tag{4}$$

Thus, the DC-link voltage u_{dc} can be derived as

$$u_{dc} = \sqrt{\frac{P_{2-peak}}{C_{dc}\omega_g}\left[K - \cos(2\omega_g t + \delta)\right]} \quad K \geq 1 \tag{5}$$

where K is the initial integral value. Figure 2a shows the waveforms of the DC-link voltage u_{dc} under different K. With the increase of K, the DC component of u_{dc} also increases, and the waveform of u_{dc} is more similar to the sinusoidal waveform.

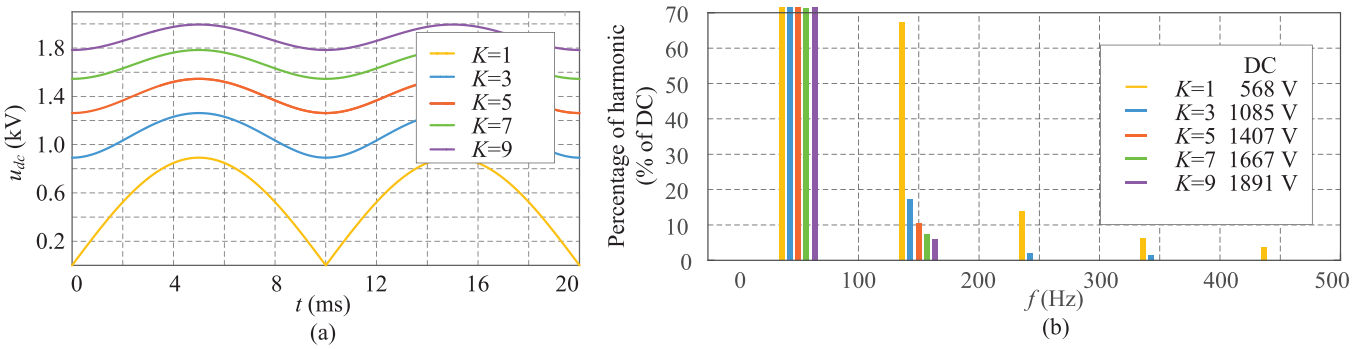

FIGURE 2 (a) The waveforms of the DC-link voltage u_{dc} under different K. (b) The harmonic spectrum of the DC-link voltage u_{dc}

According to the harmonic spectrum of the DC-link voltage u_{dc} in Figure 2b, the frequency of harmonics among u_{dc} is in the form of $2N\omega_g$, where N is an integer, and the content of these harmonics decreases as the frequency increases. When the value of K increases, the content of each harmonic decreases. And u_{dc} almost only contains the DC components and AC components at $2\omega_g$ (100 Hz) under $K > 5$.

2.2 | Phase voltage and electromagnetic torque

As the value of the DC component of u_{dc} is usually very high in EMUs (i.e. 1650 V, 3600 V), the DC-link voltage u_{dc} can be approximated as

$$u_{dc} = U_{dc} + \Delta U_{dc} \sin(2\omega_g t + \theta) \tag{6}$$

where U_{dc} and ΔU_{dc} are the amplitudes of the DC component and AC component of the DC-link voltage u_{dc}, θ is the phase angle for the AC component. The modulation index M and three-phase modulation signal m_i are defined as

$$M = \frac{U_{ref}}{U_{dc}} \tag{7}$$

$$m_i = M \cos(\omega_e t + \theta_i) \tag{8}$$

where U_{ref} is the amplitude of the phase voltage of the inverter ($M = 1.27$ under the square wave modulation mode), ω_e is the fundamental angular frequency of the motor ($\omega_e = 2\pi f_e$), $\theta_b = \theta_a - 2\pi/3$, $\theta_c = \theta_a + 2\pi/3$, and $i = a, b, c$, represent for three phases. Thus, the phase voltage of the inverter u_{ip} is derived as follows (ignoring the PWM-related harmonics):

$$\begin{aligned} u_{ip} = u_{dc} m_i = U_{dc} M \cos(\omega_e t + \theta_i) \\ + 0.5\Delta U_{dc} M \sin[(2\omega_g + \omega_e)t + \theta + \theta_i] \\ + 0.5\Delta U_{dc} M \sin[(2\omega_g - \omega_e)t + \theta - \theta_i] \end{aligned} \tag{9}$$

The phase voltage u_{ip} composes of two components: the fundamental voltage at the frequency of ω_e and the beat voltage at the beat frequency of $2\omega_g \pm \omega_e$. Therefore, the current of the motor can be derived as

$$\begin{aligned} i_i = \frac{U_{dc} M \cos(\omega_e t + \theta_i - \theta_{(\omega e)})}{Z_{(\omega e)}} \\ + \frac{\Delta U_{dc} M \sin[(2\omega_g - \omega_e)t + \theta - \theta_i - \theta_{(2\omega g - \omega e)}]}{2Z_{(2\omega g - \omega e)}} \\ + \frac{\Delta U_{dc} M \sin[(2\omega_g + \omega_e)t + \theta + \theta_i - \theta_{(2\omega g + \omega e)}]}{2Z_{(2\omega g + \omega e)}} \end{aligned} \tag{10}$$

where $Z_{(x)}$ and $\theta_{(x)}$ ($x = \omega_e, 2\omega_g - \omega_e, 2\omega_g + \omega_e$) are the amplitude and angle of the motor impedance at frequency x respectively. Based on (9) and (10), the power of the motor p_m can be expressed as (11):

$$p_m = \sum_{i=a,b,c} u_{ip} i_i = \frac{3U_{dc}^2 M^2 \cos(\theta_{(\omega e)})}{2Z_{(\omega e)}} + \frac{3\Delta U_{dc} U_{dc} M^2}{4} \left\{ \frac{\sin[2\omega_g t + \theta - \theta_{(2\omega g + \omega e)}]}{Z_{(2\omega g + \omega e)}} \frac{\sin[2\omega_g t + \theta - \theta_{(2\omega g - \omega e)}]}{Z_{(2\omega g - \omega e)}} \right\} + \frac{3\Delta U_{dc}^2 M^2}{8} \left\{ \left[\frac{\cos\theta_{(2\omega g + \omega e)}}{Z_{(2\omega g + \omega e)}} + \frac{\cos\theta_{(2\omega g - \omega e)}}{Z_{(2\omega g - \omega e)}} - \frac{\cos(4\omega_g t + 2\theta)\cos\theta_{(2\omega g + \omega e)}}{Z_{(2\omega g + \omega e)}} + \frac{\cos(4\omega_g t + 2\theta)\cos\theta_{(2\omega g - \omega e)}}{Z_{(2\omega g - \omega e)}} \right] \right\} \tag{11}$$

Ignoring the small terms with the coefficient $3\Delta U2\ dcM^2/8$ in (11) and the power loss of the motor, the electromagnetic

torque can be approximated as

$$T_e \approx \frac{p_m}{\omega} \approx \frac{U_{dc}^2 M^2}{\omega}\left(\begin{array}{l}\dfrac{3\cos(\theta_{(\omega e)})}{2Z_{(\omega e)}}+\\ \dfrac{3\Delta U_{dc}}{4U_{dc}}\left\{\begin{array}{l}\dfrac{\sin[2\omega_g t+\theta-\theta_{(2\omega g+\omega e)}]}{Z_{(2\omega g+\omega e)}}\\ +\dfrac{\sin[2\omega_g t+\theta-\theta_{(2\omega g-\omega e)}]}{Z_{(2\omega g-\omega e)}}\end{array}\right.\end{array}\right) \tag{12}$$

where ω is the electrical angular velocity of the motor. The electromagnetic torque contains a constant component that drives the motor and a pulsating component at $2\omega_g$ (100 Hz). The pulsating component is caused by the beat voltage and its amplitude is proportional to the amplitude of the fluctuating DC-link voltage and inversely proportional to the amplitude of the motor impedance at the beat frequency.

3 | BEAT-LESS ALGORITHM BASED ON DUAL-FREQUENCY COMPENSATION

3.1 | Principle of dual-frequency compensation

With the SFC method, the beat voltage at the frequency of $(2\omega_g-\omega_e)$ in (9) can be eliminated by compensating a variable related to the DC-link voltage ($\Delta U_{dc}\sin(2\omega_g+\theta)/U_{dc}$) for the three-phase output frequency [22]. However, this method will double the amplitude of the beat voltage at the frequency of $(2\omega_g+\omega_e)$. Consequently, the motor will still suffer from the beat phenomenon.

To avoid the beat voltage at the frequency of $(2\omega_g+\omega_e)$, the DFC method with two compensation variables is proposed. With the DFC method, the frequency of the modulation signal for each phase is assumed as follow:

$$\omega_{iout} = \omega_e + X_i\cos(2\omega_g t + \theta_{i1}) + Y_i\cos[(2\omega_g + 2\omega_e)t + \theta_{i2}] \tag{13}$$

where X_i and θ_{i1} are the amplitude and phase of the first compensation variable at $2\omega_g$, Y_i and θ_i are the amplitude and phase of the second compensation variable at $2\omega_g+2\omega_e$. Noted $\varphi_{ie} = \theta_i+\omega_e t$, $\varphi_{i1} = \theta_{i1}+2\omega_g t$, $\varphi_{i2} = \theta_{i2}+(2\omega_g t+2\omega_e t)$, $K_{i1} = X_i/2\omega_g$, and $K_{i2} = Y_i/(2\omega_g+2\omega_e)$, the modified modulation signal *m' id* of each phase can be derived as

$$\begin{aligned} m'_{id} &= M\cos\left[\left(\theta_i+\int\omega_{iout}dt\right)\right] \\ &= M\cos[\varphi_{ie} + K_{i1}\sin(\varphi_{i1}) + K_{i2}\sin(\varphi_{i2})] \end{aligned} \tag{14}$$

Furthermore, (14) can be resolved as

$$\begin{aligned} m'_{id} = M\cos\varphi_{ie}&\left\{\begin{array}{l}\cos[K_{i1}\sin(\varphi_{i1})]\cos[K_{i2}\sin(\varphi_{i2})]\\ -\sin[K_{i1}\sin(\varphi_{i1})]\sin[K_{i2}\sin(\varphi_{i2})]\end{array}\right\} \\ -M\sin\varphi_{ie}&\left\{\begin{array}{l}\sin[K_{i1}\sin(\varphi_{i1})]\cos[K_{i2}\sin(\varphi_{i2})]\\ +\cos[K_{i1}\sin(\varphi_{i1})]\sin[K_{i2}\sin(\varphi_{i2})]\end{array}\right\} \end{aligned} \tag{15}$$

Substituting the Bessel function (16) into (15), (17) can be obtained.

$$\left\{\begin{array}{l}\sin(x\sin\alpha) = 2\sum_{n=1,3,5...}^{\infty}J_n(x)\sin(n\alpha)\\ \cos(x\sin\alpha) = J_0(x) + 2\sum_{n=2,4,6...}^{\infty}J_n(x)\cos(n\alpha)\end{array}\right. \tag{16}$$

$$\begin{aligned} m'_{id} = M\cos\varphi_{ie}&\left\{\begin{array}{l}\left[J_0(K_{i1}) + 2\sum_{n=2,4,6...}^{\infty}J_n(K_{i1})\cos(n\varphi_{i1})\right]\\ \times\left[J_0(K_{i2}) + 2\sum_{n=2,4,6...}^{\infty}J_n(K_{i2})\cos(n\varphi_{i2})\right]\\ -\left[2\sum_{n=1,3,5...}^{\infty}J_n(K_{i1})\sin(n\varphi_{i1})\right]\\ \times\left[2\sum_{n=1,3,5...}^{\infty}J_n(K_{i2})\sin(n\varphi_{i2})\right]\end{array}\right\} \\ -M\sin\varphi_{ie}&\left\{\begin{array}{l}\left[2\sum_{n=1,3,5...}^{\infty}J_n(K_{i1})\sin(n\varphi_{i1})\right]\\ \times\left[J_0(K_{i2}) + 2\sum_{n=2,4,6...}^{\infty}J_n(K_{i2})\cos(n\varphi_{i2})\right]\\ +\left[J_0(K_{i1}) + 2\sum_{n=2,4,6...}^{\infty}J_n(K_{i1})\cos(n\varphi_{i1})\right]\\ \times\left[2\sum_{n=1,3,5...}^{\infty}J_n(K_{i2})\sin(n\varphi_{i2})\right]\end{array}\right\} \end{aligned} \tag{17}$$

where $J_0(K_{i1}) = J_0(K_{i2}) = 1, J_1(K_{i1}) = 0.5K_{i1}, J_1(K_{i2}) = 0.5K_{i2}$. In (17), $J_n(x)$ (n>1) can be omitted as they are much smaller than J_0 and J_1. Therefore, the modified modulation signal *m' id* can be simplified as

$$\begin{aligned} m'_{id} \approx{}& M\cos(\varphi_{ie})\left\{1 - K_{i1}K_{i2}\sin(\varphi_{i1})\sin(\varphi_{i2})\right\} \\ &-M\sin(\varphi_{ie})\left\{K_{i1}\sin(\varphi_{i1}) + K_{i2}\sin(\varphi_{i2})\right\} \end{aligned} \tag{18}$$

Ignoring the small-term with the coefficient $K_{i1}K_{i2}$, (18) can be further derived as

$$\begin{aligned} m'_{id} \approx{}& M\cos(\varphi_{ie}) \\ &-0.5MK_{i1}\left[\cos(\varphi_{ie}+\varphi_{i1}) - \cos(\varphi_{ie}-\varphi_{i1})\right] \\ &-0.5MK_{i2}\left[\cos(\varphi_{ie}+\varphi_{i2}) - \cos(\varphi_{ie}-\varphi_{i2})\right] \end{aligned} \tag{19}$$

3.2 | Phase voltage with dual-frequency compensation

After PWM process, the phase voltage with modified modulation signal in (19) can be derived as follows (noted $\varphi_{dc} = \theta+2\omega_g t$):

$$\begin{aligned} u_{pi} = {}& m'_{id}\,u_{dc} = MU_{dc}\cos(\varphi_{ie}) \\ &-0.5MU_{dc}K_{i1}\left[\cos(\varphi_{ie}+\varphi_{i1}) - \cos(\varphi_{ie}-\varphi_{i1})\right] \\ &-0.5MU_{dc}K_{i2}\left[\cos(\varphi_{ie}+\varphi_{i2}) - \cos(\varphi_{ie}-\varphi_{i2})\right] \\ &+M\Delta U_{dc}\sin(\varphi_{dc})\cos(\varphi_{ie}) \\ &-0.5M\Delta U_{dc}K_{i1}\left[\cos(\varphi_{ie}+\varphi_{i1}) - \cos(\varphi_{ie}-\varphi_{i1})\right]\sin(\varphi_{dc}) \\ &-0.5M\Delta U_{dc}K_{i2}\left[\cos(\varphi_{ie}+\varphi_{i2}) - \cos(\varphi_{ie}-\varphi_{i2})\right]\sin(\varphi_{dc}) \end{aligned} \tag{20}$$

where $0.5\,M\Delta U_{dc}K_{i1}$ and $0.5\,M\Delta U_{dc}K_{i2}$ are the small terms that can be ignored, thus, (20) can be decomposed and simplified as

$$
\begin{aligned}
u_{ip} \approx & \underbrace{MU_{dc}\cos(\varphi_{ie})}_{\omega_e} \\
& -\frac{MU_{dc}K_{i1}}{2}\left[\underbrace{\cos(\varphi_{ie}+\varphi_{i1})}_{2\omega_g+\omega_e}+\underbrace{\cos(\varphi_{i1}-\varphi_{ie})}_{2\omega_g-\omega_e}\right] \\
& -\frac{MU_{dc}K_{i2}}{2}\left[\underbrace{\cos(\varphi_{ie}+\varphi_{i2})}_{2\omega_g+3\omega_e}+\underbrace{\cos(\varphi_{i2}-\varphi_{ie})}_{2\omega_g+\omega_e}\right] \\
& +\underbrace{0.5M\Delta U_{dc}\cos(\varphi_{dc}+\varphi_{ie}-\frac{\pi}{2})}_{2\omega_g+\omega_e} \\
& +\underbrace{0.5M\Delta U_{dc}\cos(\varphi_{dc}-\varphi_{ie}-\frac{\pi}{2})}_{2\omega_g-\omega_e}
\end{aligned} \tag{21}
$$

It can be known that the phase voltage u_{ip} is composed of four AC components. The component at the frequency of ω_e is the fundamental voltage, the components at the frequency of $2\omega_g \pm \omega_e$ are the beat voltages that need to be eliminated, and the component at the frequency of $2\omega_g+3\omega_e$ is the harmonic voltage introduced by the DFC method. To cancel the beat voltage at the frequency of $2\omega_g \pm \omega_e$, (22) is obtained. It can be known that the amplitude of the harmonic voltage at the frequency of $2\omega_g+3\omega_e$ is $M\Delta U_d$. As such harmonic voltage is of small amplitude and high frequency, it will have little influence on the motor:

$$
\begin{cases}
\varphi_{i1}=\varphi_{dc}-\frac{\pi}{2} \\
\varphi_{i2}=\varphi_{dc}+2\varphi_{ie}-\frac{\pi}{2} \\
K_{i1}=\frac{\Delta U_{dc}}{U_{dc}} \\
K_{i2}=\frac{2\Delta U_{dc}}{U_{dc}}
\end{cases} \Rightarrow
\begin{cases}
\theta_{i1}=\theta-\frac{\pi}{2} \\
\theta_{i2}=\theta+2\theta_i-\frac{\pi}{2} \\
X_i=\frac{2\Delta U_{dc}\omega_g}{U_{dc}} \\
Y_i=\frac{4\Delta U_{dc}(\omega_g+\omega_e)}{U_{dc}}
\end{cases} \tag{22}
$$

The two compensation variables $\Delta\omega_1$ and $\Delta\omega_{i2}$ are defined as follows:

$$
\Delta\omega_1=\frac{2\Delta U_{dc}\omega_g}{U_{dc}}\sin(2\omega_g t+\theta) \tag{23}
$$

$$
\Delta\omega_{i2}=\frac{4\Delta U_{dc}(\omega_g+\omega_e)}{U_{dc}}\sin[(2\omega_g+2\omega_e)t+\theta+2\theta_i] \tag{24}
$$

3.3 | Modulation index analysis

The modified modulation signal with the SFC, DFC, and MIC methods are expressed as (25), (26), and (27), respectively. The trajectories of the modified modulation signal with these methods can be obtained by substituting (25), (26) and (27) into the space vector function (28):

$$
m'_{is}=M\cos(\theta_i+\omega_e t+\int\Delta\omega_1 dt) \tag{25}
$$

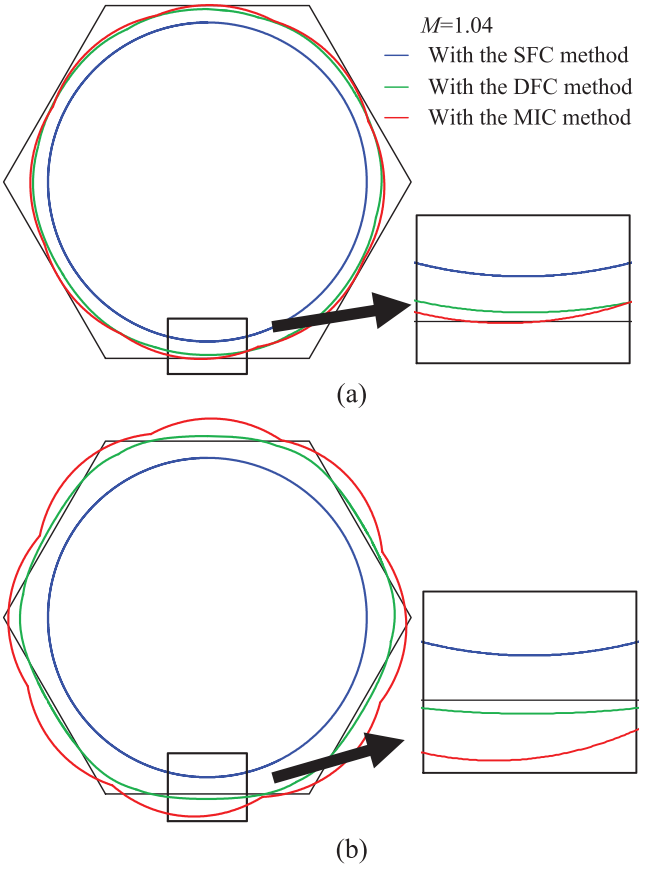

FIGURE 3 The trajectories of the modified modulation signal with different methods. (a) $\Delta U_{dc}=0.1U_{dc}$. (b) $\Delta U_{dc}=0.2U_{dc}$

$$
m'_{id}=M\cos[\theta_i+\omega_e t+\int(\Delta\omega_1+\Delta\omega_{i2})dt] \tag{26}
$$

$$
m'_{im}=\frac{MU_{dc}\cos(\omega_e t+\theta_i)}{U_{dc}+\Delta U_{dc}\sin(2\omega_g t+\theta)} \tag{27}
$$

$$
m=\frac{2}{3}\left(m_a+\lambda m_b+\lambda^2 m_c\right)\quad \lambda=e^{-j2\pi/3} \tag{28}
$$

Figure 3a shows the trajectories of the modified modulation signal with the SFC, DFC, and MIC methods while $\Delta U_{dc}=0.1U_{dc}$ and $M=1.04$. The trajectory with the SFC method is an ideal circle, which is the same as the unmodified trajectory. Thus, the SFC method has no modulation index limitation. The trajectory with the MIC method is irregular, and part of it exceeds the hexagon boundary. Therefore, overmodulation will occur, and the additional harmonics will inevitably increase. While the DFC method is adopted, the trajectory is still inside the hexagon with a certain margin.

Figure 3b shows the results while $\Delta U_{dc}=0.2U_{dc}$ and $M=1.04$. With the increase of the fluctuating DC-link voltage,

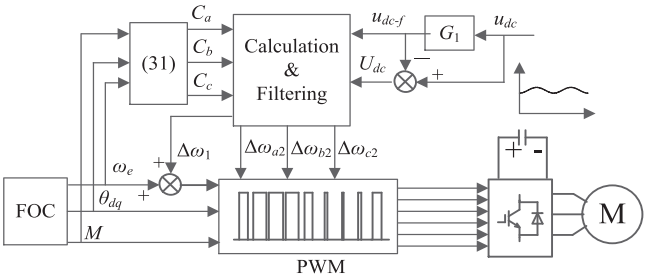

FIGURE 4 The implementation of the DFC method

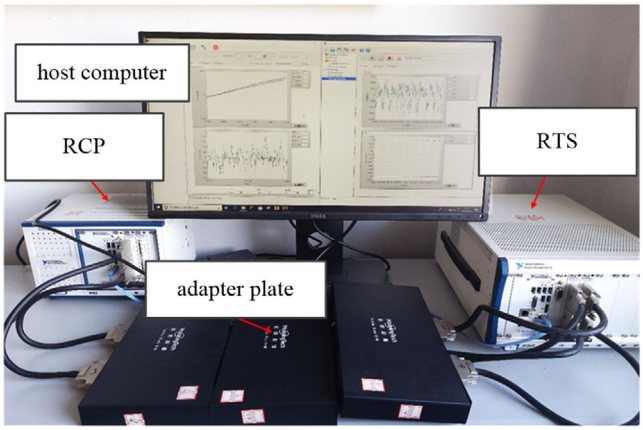

FIGURE 5 The StarSim hardware-in-loop testing platform

it can be concluded that the trajectories of the modified modulation signals with both the MIC and DFC methods are expanding outward and exceeding the hexagon boundary, resulting in overmodulation. The overmodulation phenomenon with the MIC method is much more evident than that with the DFC method. In Figure 3a and b, the trajectories of the modified modulation signals with the SFC method are always an ideal circle with a fixed radius.

Therefore, the DFC method can be a transition between the MIC and SFC methods. That is, when the modulation index is low, the MIC beat-less algorithm is used for better beat phenomenon suppression. As the modulation index increases, the trajectory is about out of the hexagon. Hence, the DFC beat-less algorithm is selected for linear modulation. As the modulation index increases further, the trajectory with the DFC method is about into the overmodulation region too. Therefore, the beat-less algorithm can be simplified as the SFC method. Consequently, the beat phenomenon can be greatly suppressed in the full speed range, thereby reducing the motor current harmonics and torque ripple.

TABLE 1 Experimental parameters

Parameters	Value
U_{dc} (V)	1650
ω_g (rad/s)	100
Motor stator leakage inductance L_{ls} (mH)	1.58
Motor stator resistance R_s (Ω)	0.223
Motor rotor leakage inductance L_{lr} (mH)	2.076
Motor rotor resistance R_r (Ω)	0.103
Motor mutual inductance L_m (mH)	43.8
Load torque T_m (N.m)	200
Control frequency of RCP f_t (Hz)	2000
Sample time of RTS t_R (μs)	1

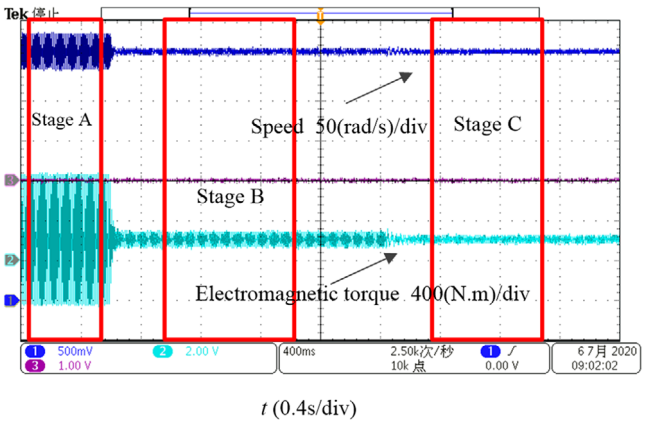

FIGURE 6 Motor speed and torque in different stages

3.4 | Implementation of dual-frequency compensation

As the analysis above, the DFC method is applied to modify the three-phase modulation signals output by the inverter-motor control strategy (filed oriented control, FOC) in PWM process, and the implementation of the DFC method is shown in Figure 4. To obtain the AC component of the DC-link voltage u_{dc} at 100 Hz, the bandpass filter $G_1(s)$ tuning at the same frequency can be used and written as follows:

$$G_1(s) = \frac{2\omega_{c1}s}{s^2 + 2\omega_{c1}s + 4\omega_g^2} \tag{29}$$

where ω_{c1} is set as 2.51 to maintain a proper bandwidth for the variation of ω_g ($\pm$0.2 Hz). As the AC component $u_{dc\text{-}f}$ is obtained by $G_1(s)$, the DC component U_{dc} can be derived by subtracting $u_{dc\text{-}f}$ in u_{dc}. Therefore, the first compensation variable $\Delta\omega_1$ can be expressed as

$$\Delta\omega_1 = \frac{2\omega_g u_{dc-f}}{U_{dc}} \tag{30}$$

For the calculation of the second compensation variable $\Delta\omega_{i2}$, two temporary variables C_i and D_i are defined as follows:

$$C_i = \sin(\omega_e t + \theta_i) \tag{31}$$

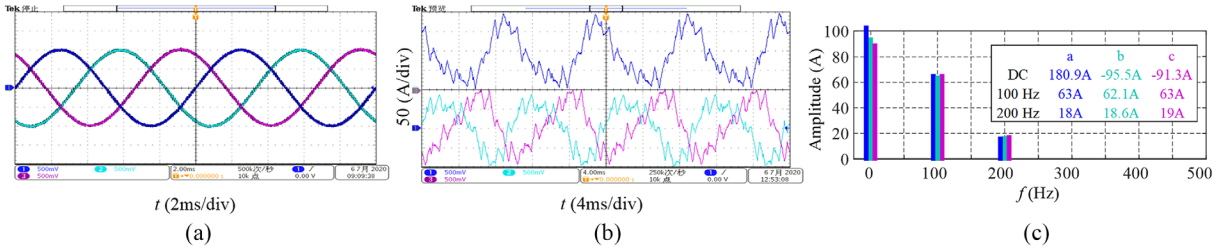

FIGURE 7 Without any method in stage A. (a) The modulation signals. (b) Three-phase currents of the motor. (c) The harmonic spectrum of the currents

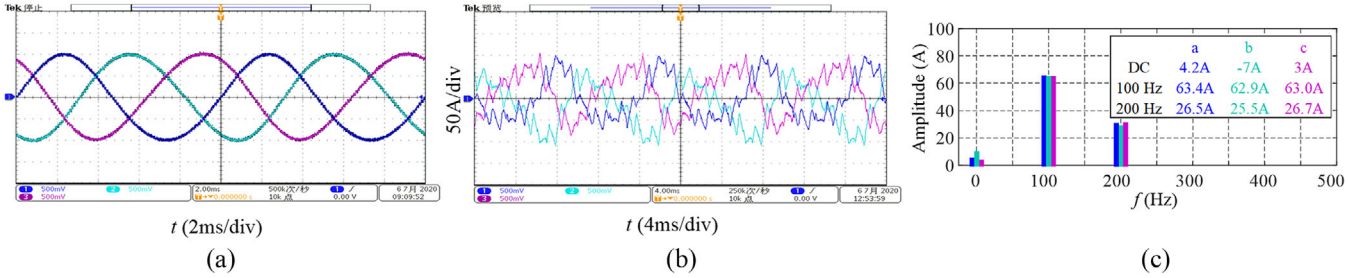

FIGURE 8 With the SFC method in stage B. (a) The modulation signals. (b) Three-phase currents of the motor. (c) The harmonic spectrum of the currents

$$D_i = \frac{8(1-2C_i^2)(\omega_g+\omega_e)u_{dc-f}}{U_{dc}} = \frac{4\Delta U_{dc}(\omega_g+\omega_e)}{U_{dc}} \begin{pmatrix} \sin[(2\omega_g + 2\omega_e)t + \theta + 2\theta_i] \\ + \sin[(2\omega_g - 2\omega_e)t + \theta - 2\theta_i] \end{pmatrix} \tag{32}$$

The bandpass filter $G_2(s)$ is used to extract the component with the frequency of $2\omega_g+2\omega_e$ in (32) and written as follows:

$$G_2(s) = \frac{2\omega_{c2}s}{s^2 + 2\omega_{c2}s + 4(\omega_g + \omega_e)^2} \tag{33}$$

where ω_{c2} is also set as 2.51 to maintain a proper bandwidth for the variation of ω_g ($\pm$0.2 Hz). Thereby, after the filtering process, the second compensation variable $\Delta\omega_{i2}$ is obtained.

4 | EXPERIMENTS RESULTS

The StarSim hardware-in-loop testing platform is used for experimental verification. The platform, shown in Figure 5, consists of a host computer, an adapter plate, a rapid control prototype (RCP), and a real-time simulator (RTS). The FOC strategy and beat-less algorithm run on RCP, while the inverter-motor system model is executed in RTS in real-time. RCP and RTS are connected through actual physical IO to transmit signals. The control commands are sent by the host computer. The experimental parameters are shown in TABLE I, ΔU_d is set as 165 V. The fundamental frequency f_e is 100 Hz with a switching frequency of 1000 Hz to simulate the beat phenomenon in the worst conditions.

In Figure 6, the experiment is carried out in three stages. There is no beat-less method in stage A, while the SFC and DFC methods are applied to stages B and C respectively. It can be seen that the speed and torque both fluctuate significantly in stage A, and the amplitude of torque pulsation is higher than 600 N·m. After the SFC method is used, the pulsations of the speed and torque are suppressed. The amplitude of the torque pulsation drops to about 100 N·m, shown in stage B. The speed and torque are becoming smoother with the DFC method, and the amplitude of the torque pulsation is only about 50 N·m shown in stage C.

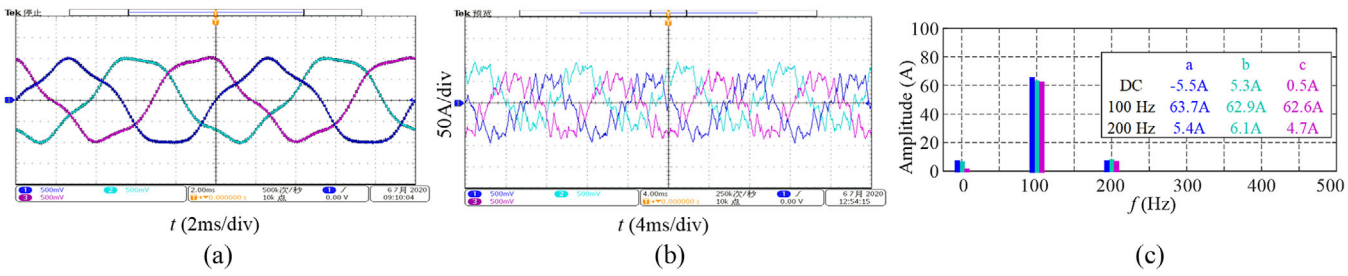

FIGURE 9 With the DFC method in stage C. (a) The modulation signals. (b) Three-phase currents of the motor. (c) The harmonic spectrum of the currents

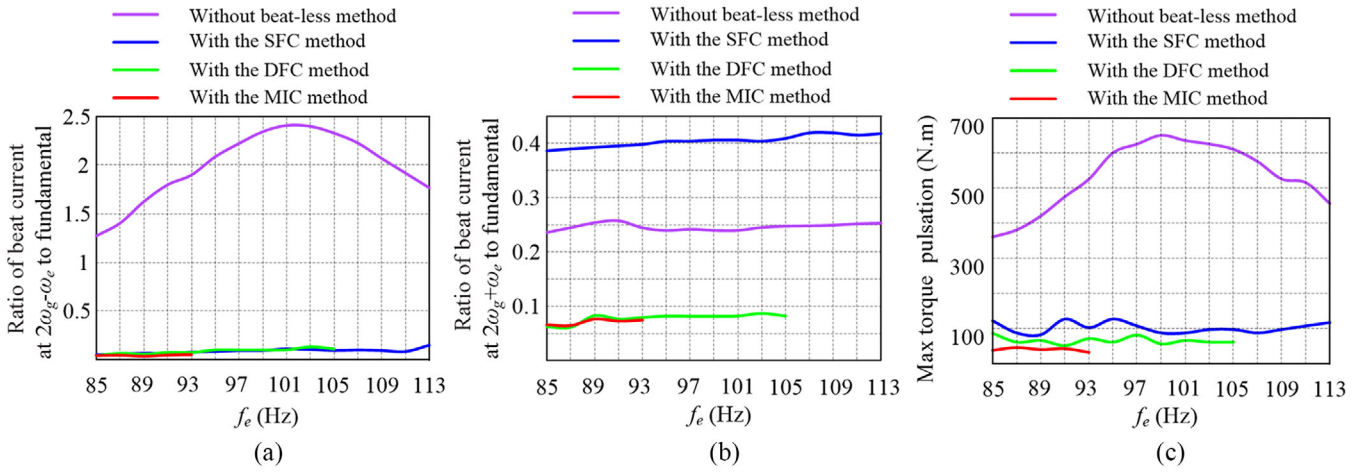

FIGURE 10 The comparison results with different methods while $\Delta U_{dc} = 0.1 U_{dc}$. (a) The low-frequency beat current comparison. (b) The high-frequency beat current comparison. (c) The max torque pulsation comparison

The three-phase modulation signals, the waveforms and the harmonic spectrum of the motor current in different stages are shown in Figures 7, 8, and 9 respectively. In stage A as shown in Figure 7, the modulation signals are symmetrical sinusoidal. Under such modulation signals, the beat voltage occurs, leading to the asymmetric current obviously. The low-frequency beat current ($2\omega_g - \omega_e$, which is 0 Hz) for phase *a* reaches as high as 180.9 A, while they are -95.5 A and -91.3 A for phase *b* and *c* respectively. The high-frequency beat-current ($2\omega_g + \omega_e$, which is 200 Hz) for three phases are almost the same with the value ranging from 18 to 19 A.

Figure 8 shows the results of the SFC method in stage B. The modulation signals are modified and distorted slightly, but they are still of three-phase symmetry. the DC component of the three-phase current drops significantly to 4 A, 4 A, and 12 A respectively. The high-frequency beat-current has increased by about 8 A.

With the DFC method, the beat phenomenon is suppressed more effectively, shown in Figure 9. A notable feature of the DFC method is that the modified modulation signals are obviously distorted and no longer three-phase symmetrical. Consistent with the analysis above, the beat currents at frequencies of $2\omega_g \pm \omega_e$ are eliminated. The waveforms of the three-phase currents can be more symmetrical compared with the waveforms in Figure 8b. It should be noted that the currents in Figure 7b, Figure 8b, and Figure 9b are rich in the PWM-related harmonics due to the low switching frequency.

To further test the performance of the SFC, DFC, and MIC methods, the comparison experiments among them are carried out while f_e is ranged from 85 to 113 Hz. The carrier ratio (f_s/f_e) is set as 10 for synchronous modulation. The results are shown in Figure 10 while $\Delta U_{dc} = 0.1 U_{dc}$. Based on the FOC strategy, the modulation index increases as f_e increases, thus, the motor can operate at rated flux. The results in Figure 10 show the valid speed range of different beat-less algorithms. When f_e is higher than 93 Hz, the trajectory of the modified modulation signal with the MIC method is out of the linear modulation region. As for the DFC method, the linear modulation still can be realized until f_e is higher than 105 Hz. In the region where f_e exceeds 105 Hz, only the SFC method can be applied for beat phenomenon suppression. Figure 10a gives the low-frequency beat currents comparison results with different beat-less algorithms. When f_e is closed to 100 Hz, the ratio of the low-frequency beat currents reaches its peak if the beat-less algorithm is not applied. The reason for that can be explained by the motor impedance characteristic [22]. After the beat-less algorithm is used, the ratio of low-frequency beat current can be reduced significantly. Figure 10b shows the ratio of the high-frequency beat current. As the SFC method is used, more high-frequency beat currents will be introduced. On the contrary, The MIC and DFC methods can suppress the high-frequency beat current effectively with almost the same performance. The comparison of max torque pulsation is shown in Figure 10c. Without any beat-less algorithm, the peak value of max torque pulsation can be obtained at 100 Hz due to the high value of the low-frequency beat current. The torque pulsation can be suppressed by these three beat-less algorithms. Some small terms in (9), (18), (19), and (20) are ignored in the calculation process. Besides, the principle of the DFC method is to shift the beat voltages to a higher-frequency region, rather than cancel them out. All these factors result in worse performance for torque pulsation suppression compared with the MIC method. However, the torque pulsation suppression effect with the DFC method can still be better than that with the SFC method, because the high-frequency beat current is also eliminated by the DFC method.

Figure 11 also presents the comparison results while $\Delta U_{dc} = 0.2 U_{dc}$, which are almost the same as the results in Figure 10. However, all indexes (including the rates of the low and high-frequency beat currents, the max torque pulsation) in Figure 11 are higher than these in Figure 10 due to the larger DC-link voltage ripple. In Figure 11, the maximum f_e for the linear modulation with the MIC and DFC method are 87 and 103 Hz respectively, which both become smaller compared with Figure 10. However, for the DFC method, the applicable linear modulation region is 12 Hz (107–93 Hz) in Figure 10, whereas it is 16 Hz (103–87 Hz) in Figure 11. Therefore, the

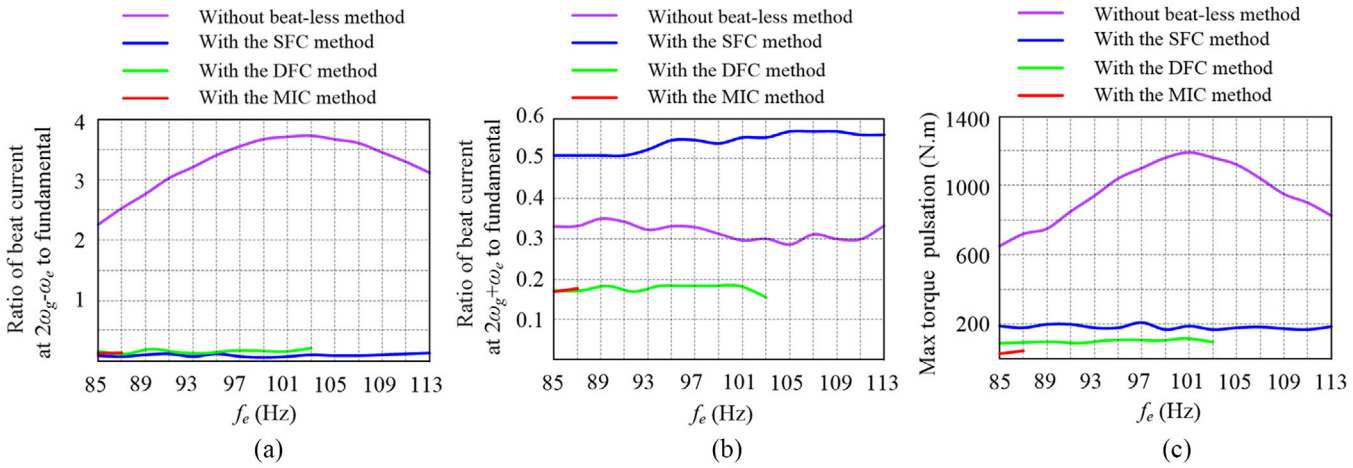

FIGURE 11 The comparison results with different methods while $\Delta U_{dc} = 0.2U_{dc}$. (a) The low-frequency beat current comparison. (b) The high-frequency beat current comparison. (c) The max torque pulsation comparison

applicable modulation range for the DFC method can be higher with a larger DC-link voltage fluctuation.

5 | CONCLUSION

In this paper, the beat-less algorithm based on the DFC method is proposed to shift the spectrum of the beat voltage to a higher-frequency region. Two variables are used for frequency compensation, thereby, both the low and high-beat currents can be eliminated. As the DFC method can be applied under a higher modulation index than the MIC method and has a better beat phenomenon than the SFC method, it can be the transition between the MIC and SFC. Consequently, the traction performance of the EMUs can be improved in the full speed range. The implementation of DFC gives guidance on how to obtain the two variables. The applicability and superiority of the DFC method are verified by the StarSim hardware-in-the-loop platform.

ORCID

Lailai Shen https://orcid.org/0000-0002-2881-2014
Jie Chen https://orcid.org/0000-0001-9259-8270
Dao Zhou https://orcid.org/0000-0001-9531-4309
Chao Wu https://orcid.org/0000-0003-0181-4738
Zhigang Liu https://orcid.org/0000-0003-3054-1425

REFERENCES

1. Hill, R.J.: Electric railway traction. Part 2: Traction drives with three-phase induction motors. Power Eng. J. 8(3), 143–152 (1994)
2. Zhao, S., et al.: DC-link-fluctuation-resistant predictive torque control for railway traction permanent magnet synchronous motor in the six-step operation. IEEE Trans. Power Electron. 35(10), 10982–10993 (2020)
3. Zhao, N., et al.: Beat phenomenon suppression for reduced DC-link capacitance IPMSM drives with fluctuated load torque. IEEE Trans. Ind. Electron. 66(11), 8334–8344 (2019)
4. Chang, G.W., et al.: Modeling characteristics of harmonic currents generated by high-speed railway traction drive converters. IEEE Trans. Power Delivery 19(2), 766–773 (2004)
5. Ronanki, D., Williamson, S.S.: Submodule power balancing control of modular multilevel converters under capacitor degradation. IET Power Electron. 13(14), 3032–3043 (2020)
6. Goodarzi, A., et al.: Multi-criteria protection scheme for online element failure detection in shunt capacitor banks. IET Gener. Transm. Distrib. 14(19), 4152–4163 (2020)
7. Song, W., et al.: One-cycle control of induction machine traction drive for high speed railway—Part I: Multi-pulse width modulation region. In: Proceeding 36th Annual Conference on IEEE Industrial Electronics Society, Glendale, AZ, USA, 7–10 Nov. 2010
8. Song, W., et al.: One-cycle control of induction machine traction drive for high speed railway—Part II: Square wave modulation region. In: Proceeding 26th Annual IEEE Applied Power Electronics Conference, Fort Worth, TX, USA, 6–11 March 2011
9. Diao, L., et al.: An efficient DSP–FPGA-based implementation of hybrid PWM for electric rail traction induction motor control. IEEE Trans. Power Electron. 33(4), 3276–3288 (2018)
10. Zhang, H., et al.: Smooth transition of multimode synchronous modulation for IPMSM sensorless drives in rail-transit applications. IEEE Trans. Ind. Electron. 68(1), 128–138 (2021)
11. de Oliveira Filho, M.E., et al.: A control method for voltage source inverter without DC link capacitor. In Proceeding IEEE Power Electronics Specialists Conference, Rhodes, Greece, 15–19 June 2008
12. Shi, W., et al.: A new method based on PIR controller to reject torque and current ripple under fluctuating DC voltage for high-speed train traction drives. In: 15th Proceeding International Conference Electrical Machines Systems, Sapporo, Japan, 21–24 Oct. 2012
13. Li, G., Zheng, et al.: Multi-mode SHEPWM with low switch frequency for traction application. In: Proceeding 19th European Conference on Power Electronics and Applications, Warsaw, Poland, 11–14 Sept. 2017
14. Kikuchi, T., et al.: Current compensation method for sensorless controlled induction motors operated in low switching frequency. In: Proceeding 15th International Conference Electronics Machines and Systems, Sapporo, Japan, 21–24 Oct. 2012
15. Ouyang, H., et al.: Repetitive compensation of fluctuating DC link voltage for railway traction drives. IEEE Trans. Power Electron. 26(8), 2160–2171 (2011)
16. Lee, J.Y., Sun, Y.Y.: Adaptive harmonic control in PWM inverters with fluctuating input voltage. IEEE Trans. Ind. Electron. IE-33(1), 92–98 (1986)
17. Diao, L.J., et al.: Ripple analysis and control of electric multiple unit traction drives under a fluctuating DC link voltage. J. Power Electron. 16(5), 1851–1860 (2016)
18. Ge, X., et al.: Beatless control technology and its application in three-level inverter. In: Proceeding International Conference on Electrical Machines Systems, Wuhan, China, 17–20 Oct. 2008

19. Kimura, A.: Frequency domain analysis of beatless control method for converter-inverter driving systems applied to AC electric cars. IEEE Trans. Ind. Appl. 128(11), 1269–1274 (2008)
20. Enjeti, P.N., Shireen, W.: A new technique to reject DC-link voltage ripple for inverters operating on programmed PWM waveforms. IEEE Trans. Power Electron. 7(1), 171–180 (1992)
21. Kouro, S., et al.: Multicarrier PWM with DC-link ripple feedforward compensation for multilevel inverters. IEEE Trans. Power Electron. 23(1), 52–59 (2008)
22. Gou, B., et al.: Analysis and compensation of beat phenomenon for railway traction drive system fed with fluctuating DC-link voltage. In: Proceeding of the 7th International Power Electronics and Motion Control Conference, Harbin, China, 2–5 June 2012
23. Lei, Y., et al.: An improved beatless control method of AC drives for railway traction converters. In: Proceeding International Conference on Electrical Machines Systems, Chiba, Japan, 13–16 Nov. 2016
24. Park, J.H., et al.: Control method of propulsion control device for AC railway vehicle. In Proceeding Transportation Electrification Conference and Expo, Busan, Korea (South), 1–4 June 2016
25. Nakata, K., et al.: A beatless control of inverter-induction motor system driven by a rippled DC power source. Electr. Eng. Japan 109(5), 122–131 (1989)

How to cite this article: Shen, L., et al.: Beat-less algorithm based on dual-frequency compensation in railway traction applications. IET Power Electron. 14, 1985–1994 (2021). https://doi.org/10.1049/pel2.12164